Biochemistry and Biophysics Reports 38 (2024) 101686

Contents lists available at ScienceDirect

Biochemistry and Biophysics Reports

journal homepage: www.elsevier.com/locate/bbrep

Blockage of αvβ3 integrin in 3D culture of triple-negative breast cancer and endothelial cells inhibits migration and discourages endothelial-to-mesenchymal plasticity

Bruna Carla Casali [a,b], Matheus Pintor Baptista [a,c], Bianca Cruz Pachane [a], Anelise Abreu Cortez [a], Wanessa Fernanda Altei [a,d,e], Heloísa Sobreiro Selistre-de-Araújo [a,*]

[a] Biochemistry and Molecular Biology Laboratory, Universidade Federal de São Carlos - UFSCar, São Carlos, SP, Brazil
[b] Brazilian Biosciences National Laboratory (LNBio), Brazilian Center for Research in Energy and Materials (CNPEM), Campinas, SP, Brazil
[c] Brazilian Nanotechnology National Laboratory (LNNano), Brazilian Center for Research in Energy and Materials (CNPEM), Campinas, SP, Brazil
[d] Radiation Oncology Department, Barretos Cancer Hospital, Barretos, SP, Brazil
[e] Center of Molecular Oncology Research, Barretos Cancer Hospital, Barretos, SP, Brazil

ARTICLE INFO

Keywords:
3D culture
$\alpha_v\beta_3$ integrin
Cell migration
Triple-negative breast cancer
Endothelial cell

ABSTRACT

Breast cancer is a relevant cause of mortality in women and its triple-negative subtype (TNBC) is usually associated with poor prognosis. During tumor progression to metastasis, angiogenesis is triggered by the sprouting of endothelial cells from pre-existing vessels by a dynamic chain of events including VE-cadherin downregulation, actin protrusion, and integrin-mediated adhesion, allowing for migration and proliferation. The binding of tumoral and tumor-associated stromal cells with the extracellular matrix through integrins mediates angiogenic processes and certain integrin subtypes, such as the $\alpha_v\beta_3$ integrin, are upregulated in hypoxic TNBC models. Integrin $\alpha_v\beta_3$ inhibition by the high-affinity binding disintegrin Dis*Ba*-01 was previously demonstrated to induce anti-tumoral and anti-angiogenic responses in traditional 2D cell assays. Here, we investigate the effects of integrin $\alpha_v\beta_3$ blockage in endothelial and TNBC cells by Dis*Ba*-01 in 3D cultures under two oxygen conditions (1% and 20%). 3D cultures created using non-adhesive micromolds with Matrigel were submitted to migration assay in Boyden chambers and fluorescence analysis. Dis*Ba*-01 inhibited cell migration in normoxia and hypoxia in both MDA-MB-231 and HUVEC spheroids. Protein levels of integrin $\alpha_v\beta_3$ were overexpressed in HUVEC spheroids compared to MDA-MB-231 spheroids. In HUVEC 3D cultures, sprouting assays in collagen type I were decreased in normoxia upon Dis*Ba*-01 treatment, and VE-cadherin levels were diminished in HUVEC spheroids in hypoxia and upon Dis*Ba*-01 treatment. In conclusion, the blockage of integrin $\alpha_v\beta_3$ by Dis*Ba*-01 inhibits cell migration in 3D culture and interferes with tumor-derived responses in different oxygen settings, implicating its crucial role in angiogenesis and tumor progression.

1. Introduction

Breast cancer is the main neoplasia in women, corresponding to 31% of diagnoses and 15% of deaths by cancer (Siegel et al., 2023). These solid tumors can be categorized according to multiple molecular characteristics and one of such accounts for their expression of hormonal receptors for estrogen (ER), progesterone (PR), and human epidermal growth factor type 2 (HER2), whose profiling aids targeted therapy (Jackson et al., 2020; Kashyap et al., 2022). The absence of all three receptors comprises the triple-negative breast cancer (TNBC) subtype, which is insensitive to hormonal therapy and subsequently becomes a more aggressive tumor prone to metastasis (Derakhshan and Reis-Filho, 2022).

Angiogenesis is a hallmark of tumor growth and metastasis (Hanahan, 2022). This process generates new blood vessels from the pre-existing vasculature, triggered by the secretion of vascular endothelial growth factor (VEGF) overcoming anti-angiogenic factors. VEGF is secreted by cells from the tumor microenvironment and binds to its receptor, VEGFR2, to promote the sprouting of quiescent endothelial cells (Ahmad and Nawaz, 2022). Endothelial cells create dynamic interconnections via the remodeling of surface proteins such as the vascular endothelial (VE) -cadherin, a transmembrane molecule that

* Corresponding author.
E-mail address: hsaraujo@ufscar.br (H.S. Selistre-de-Araújo).

https://doi.org/10.1016/j.bbrep.2024.101686
Received 8 January 2024; Received in revised form 8 March 2024; Accepted 12 March 2024

constitutes adherent junctions and is crucial for vascularization (Giannotta et al., 2013; Heiss et al., 2015). VE-cadherin expression is lost during the plastic phenotype modifications that culminate in the endothelial-to-mesenchymal transition (EndMT), marking the invasive stages of cancer, and may be related to resistance to chemotherapy ([1]; Piera-Velazquez and Jimenez, 2019). The interplay between VEGF secretion and VE-cadherin switch for endothelial cell migration and proliferation is essential for tumor progression (Wallez et al., 2006).

In solid tumors, the accelerated growth of the tumor mass promotes the development of under-nourished and hypoxic areas, which stimulates the expression of collagen type I and may lead to fibrosis and increased extracellular matrix (ECM) stiffness (Petrova et al., 2018). Hypoxia impairs the hypoxia-inducible factor (HIF) pathway function in balancing oxidative and glycolytic metabolism (Wicks and Semenza, 2022). As a consequence, it increases the transcription of genes that induce angiogenesis (i.e., VEGF), endothelial cell migration, and proliferation (Madu et al., 2020; Petrova et al., 2018).

The ECM is also a critical factor in tumor structure and function (Najafi et al., 2019). Depending on its stiffness and composition, it may drive intracellular signals through a set of accessory proteins including kinases that lead to cell migration, proliferation, and invasion (Hamidi and Ivaska, 2018; Najafi et al., 2019). These signals are carried mostly through integrins, a family of 24 heterodimeric receptors formed by the combination of 18 alpha and 8 beta subunits, comprising an extracellular domain binding to ECM components, and an intracellular tail connected with the actin cytoskeleton (Hamidi and Ivaska, 2018). Cancer-derived hypoxia is known to upregulate integrin subunits β_1 in fibroblasts, β_2 in leukocytes, β_3 and α_5 in breast tumor cells, and dimers $\alpha_v\beta_5$ and $\alpha_v\beta_3$ in endothelial cells (Ju et al., 2017; Keely et al., 2009; Kong et al., 2004; Walton et al., 2000).

In particular, integrin $\alpha_v\beta_3$ binds to ECM proteins that contain an RGD motif, such as vitronectin and fibronectin, to coordinate cell migration, invasion, and focal adhesions which may elicit downstream processes including angiogenesis and metastasis (Mezu-Ndubuisi and Maheshwari, 2021; Shattil et al., 2010). Its blockage by Cilengitide, a cyclic peptide containing an RGD motif, elicited a strong immune response in melanoma cells and became promising in cancer therapy during pre-clinical trials (Haddad et al., 2017; Pan et al., 2022). *In vitro* and *in vivo* studies with Dis*Ba*-01, an RGD recombinant disintegrin derived from the *Bothrops alternatus* snake venom, have shown its anti-tumor and anti-angiogenic potential [2–5]. A recent study from our group demonstrated that higher concentrations of Dis*Ba*-01 are required to inhibit 2D cell migration of TNBC cells in hypoxia rather than normoxia [2]. Here we upscale this investigation by using a three-dimensional model to mimic the tumor microenvironment in terms of oxygenation and drug distribution. Our work proposes to understand the role of $\alpha_v\beta_3$ integrin inhibition with Dis*Ba*-01 in 3D cell cultures of MDA-MB-231 and HUVEC cells, following up on previous 2D studies from our group.

2. Materials and methods

2.1. 2D cell culture

Triple-negative breast adenocarcinoma cells (MDA-MB-231, ATCC® HTB-26™) and human umbilical vein endothelial cells (HUVEC, ATCC® CRL-1730™) were cultured in Dulbecco's modified Eagle's medium (DMEM, Vitrocell) supplemented with 10% (v/v) of fetal bovine serum (FBS, Vitrocell), penicillin (100 IU/ml) and streptomycin (100 mg/ml, Vitrocell), and L-glutamine (2 mM), in a humidified incubator at 37 °C and 5% CO_2. HUVECs were maintained from passages 8 to 20.

2.2. Generation of spheroids

Sterile silicone micro-molds (MicroTissue 3D Petri Dish micro-mold, Sigma Z764019) were used to form ultrapure agarose (20 mg/ml in 0.9% NaCl) scaffolds, which were washed with saline buffer (PBS) and equilibrated with 3D-culture medium, i.e. complete DMEM medium supplemented with ascorbic acid (50 μg/ml), human albumin (1.25 μg/ml), 1x ITS (insulin, transferrin and selenium), and growth factor-reduced Matrigel (7%, Corning #354230). Cells were plated onto micromolds in 3D-culture medium and incubated for 7 days at 37 °C, 5% CO_2 for spheroid formation. Wide field images of three areas per well were obtained in an inverted microscope (Axio Vert.A1, Carl Zeiss) using the AxioVision Rel.4.8 software (Carl Zeiss) under 10x magnification for morphology characterization. 3D cultures were maintained at 37 °C under normoxic (~20% O_2, 5% CO_2) or hypoxic (1% O_2, 5% CO_2; H35 Hypoxystation, Don Whitley Sci.) atmospheres.

2.3. Transwell migration assay

Boyden chambers were assembled with transwell inserts (ThinCert™ translucent PET membrane, 8.0 μm pore, Greiner Bio-one®) in 24 well plates. Dis*Ba*-01 was produced as previously described [5]. Spheroids were transferred from molds to microtubes and treated with Dis*Ba*-01 (10, 100, 1000, or 2000 nM) in serum-free medium, for 30 min at room temp, and assembled on the upper compartment of the migration chamber that contained DMEM 10% FBS at the bottom compartment for 24 h at 37 °C under normoxic or hypoxic conditions. Spheroids were retrieved from the upper chamber with a PBS gush and prepared for immunofluorescence. Excess cells from the upper chamber were removed with a cotton swab. Migrated cells were fixed with 3.7% paraformaldehyde (PFA-H_2O) for 10 min at room temp, washed twice with PBS, and stained with DAPI (0.7 ng/μl, Thermo Fisher #62248) for 10 min at room temp. Membranes were assembled onto a microscope slide for fluorescent imaging at 10x magnification (ImageXpress Micro XRS, Molecular Devices; InCell Analyser 2200, GE Healthcare; Vert.A1, Carl Zeiss). Automated cell counting was performed using the "multi-wavelength cell scoring" module on the MetaXpress software (Molecular Devices), or the "analyze particle" module for ImageJ software (v.1.52a).

2.4. Immunofluorescence

HUVECs were seeded (10^5 cells) on 12 mm glass coverslips (Exacta) added to 24-well plates and incubated at 37 °C and 5% CO_2 for 24 h Cells were treated with Dis*Ba*-01 and incubated for 24 h in normoxic or hypoxic conditions. Spheroids were pelleted at 1200 rpm for 5 min, washed in PBS (1200 rpm, 5 min), and resuspended in 3% BSA-PBS for placement in a silanized glass slide. Samples were fixed for 20 min with 4% PFA-PBS, washed twice with PBS, and permeabilized with 0.3% Triton X-100 for 10 min at room temp. Samples were neutralized with 0.1 M glycine for 5 min and blocked with 3% BSA-PBS for 1 h. Primary antibodies were diluted in 3% BSA-PBS and incubated for 1 h at room temp or overnight at 4 °C. Spheroids were probed for integrin $\alpha_v\beta_3$ (1:500, Abcam #78289) and collagen type I (1:500, Abcam #130805), while HUVECs were probed for VE-cadherin (1:70, Thermo Fisher Scientific #36–1900). After washing, secondary antibodies were incubated for 1 h at room temp (Goat Anti-Rabbit IgG H&L-FITC, 1:1000, Abcam #6785; Goat Anti-Rabbit IgG H&L-APC, 1:500, Abcam #130805; Goat anti-Rabbit IgG (H + L) A488, 4 μg/ml, Thermo Fisher Scientific #A11008). Excess stain was removed and nuclei were stained with DAPI for 20 min. After washes, samples were assembled using Prolong Diamond Antifade Mounting Media (Invitrogen) and imaged using confocal laser scanning microscopy (Fluoview FV10, Olympus) under 63x magnification and 2× optical zoom. Laser intensity was maintained throughout acquisitions. Image processing was performed using FIJI (SCHINDELIN, 2012), using the "3D viewer" plugin for nuclei count and the threshold tool for quantification of fluorescence intensity for integrin $\alpha_v\beta_3$ and collagen type I. Secondary antibody control was used as a normalizer. VE-cadherin fluorescence quantification was calculated using the "branch length" tool from the "Skeleton" plugin as (branch

length)/(nuclei count).

2.5. Sprouting assay

Following a previous method (HEISS 2015), spheroids were ejected from the mold with a PBS gush, centrifuged at 1200 rpm for 5 min, washed with PBS, and re-spun. They were resuspended in DMEM (100 μl) mixed with collagen type I (1.2 mg/ml, BD Biosciences #354236) and treated with Dis*Ba*-01 (1000 nM, 24, 48 and 72 h). Spheroids were seeded in a 96-well plate and incubated at 37 °C, 5% CO_2. After col type I polymerization, spheroids were stimulated with 3D-culture media for 72 h. Widefield images were obtained after 24, 48, and 72 h under 10x magnification using the inverted microscope Axio Vert.A1 coupled with the AxioVision Rel.4.8 software (Carl Zeiss). The average length of sprouts was obtained as the (sum of the length of sprouts)/(number of sprouts in each spheroid).

2.6. Statistical analysis

Data were obtained from three independent experiments performed in three technical replicates and analyzed on the software SigmaPlot (v.12). For parametric data, we performed two-way ANOVA or one-way ANOVA with Tukey's *post hoc* test, and non-parametric data were subjected to the Kruskall–Wallis one-way analysis of variance on ranks with Dunn's *post hoc* test. Values of $p < 0.05$ were considered statically significant. Graphs showing mean ± SD or median ± SD depending on data distribution were assembled using GraphPad Prism (v.8).

3. Results

3.1. Characterization of three-dimensional cell culture of MDA-MB-231 and HUVEC lines

For the formation of spheroids from MDA-MB-231, 5×10^5 cells were added to molds and generated masses with diameters of 409.4 ± 37.46 μm after one day, 404.2 ± 66.28 μm after three days, and 486.2 ± 100.6 μm after six days (Fig. 1A). The diffuse border morphology and general characteristics of the spheroids are consistent with a compact aggregate (Fig. 1B). Upon immunostaining, tumoral spheroids showed a diffuse and more central distribution of collagen type I and integrin $\alpha_v\beta_3$, indicating secretion of extracellular matrix and its interaction with cells (Fig. 1C).

In HUVECs, a higher number of cells was required to achieve spheroid formation, at 1×10^6 cells per mold. Cell clusters reached diameters of 438.1 ± 35.45 μm after one day, 390.9 ± 34.90 μm after three days, and 396.0 ± 32.08 μm after six days (Fig. 1D), and visual inspection of structures indicated a tight perimeter and dense mass typical of compact spheroids (Fig. 1E). Under confocal microscopy, we observe the structures have well-marked borders, with high peripheral expression of integrin $\alpha_v\beta_3$ and collagen type I (Fig. 1F).

3.2. Blockage of integrin $\alpha_v\beta_3$ by DisBa-01 inhibits cell migration from spheroids

Since Dis*Ba*-01 inhibits HUVEC chemotactic migration (DANILUCCI 2018) and impairs MDA-MB-231 cell migration (CASALI 2022; MONTENEGRO 2017), we investigated whether similar behaviors also occurred in a 3D cell culture setting. In compact aggregates from MDA-MB-231, Dis*Ba*-01 reduced migration at 10 nM (66.13%, $p < 0.05$), 100 nM (38.6%), and 1000 nM (70.75%, $p < 0.05$) under normoxia conditions. In hypoxia conditions, migration inhibition at 10 nM (57.35%, $p < 0.05$), 100 nM (32.15%), and 1000 nM (55.83%, $p < 0.05$) were observed (Fig. 2A). Representative images of the disposition of migrating cells in a porous membrane during the chemotactic assay is displayed in Fig. 2B. In compact spheroids from HUVEC, Dis*Ba*-01 was also efficient in inhibiting chemotactic migration under hypoxic and normoxic conditions. Dis*Ba*-01 inhibited migration in normoxia at 100 nM (50.91%, $p < 0.05$), 1000 nM (57.95%, $p < 0.05$), and 2000 nM (75.68%, $p < 0.05$), and in hypoxia at 100 nM (73.72%, $p < 0.05$), 1000 nM (84.97%, $p < 0.05$), and 2000 nM (84.5%, $p < 0.05$). Untreated cells in hypoxia also showed a significant reduction in migration compared to the untreated control in normoxia (Fig. 2C). Cell density in membranes after 24 h of migration is displayed in Fig. 2D.

3.3. Collagen type I and integrin $\alpha_v\beta_3$ differential expression in spheroids from MDA-MB-231 and HUVEC

Integrin $\alpha_v\beta_3$ expression and collagen type I secretion profiles in spheroids from MDA-MB-231 and HUVEC were obtained from an immunofluorescence assay under normoxic and hypoxic conditions.

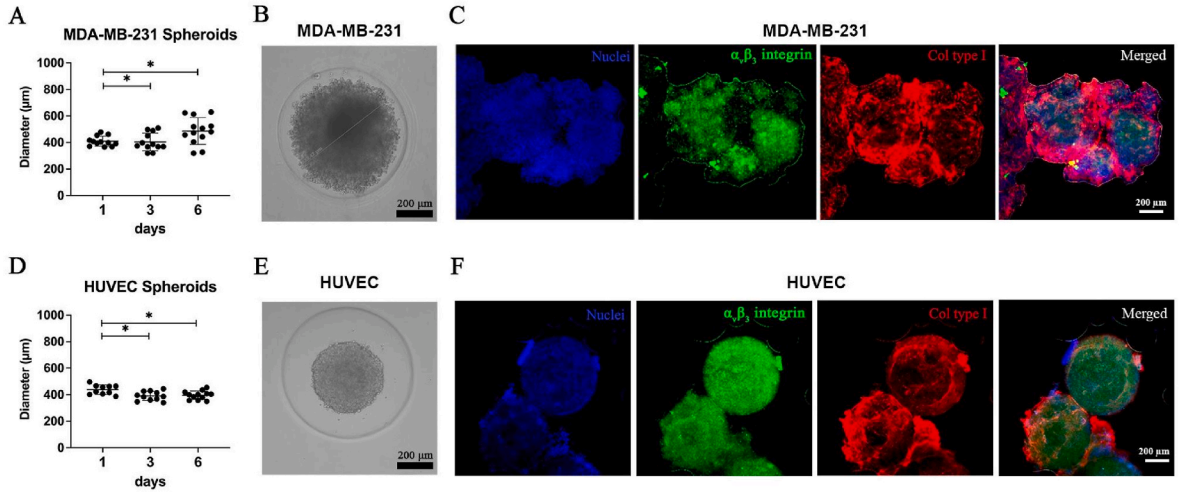

Fig. 1. Characterization of spheroids from MDA-MB-231 and HUVEC cell lines. (A) Diameter of MDA-MB-231 spheroids originated from 5×10^5 cells per mold after 1, 3, and 6 days of incubation. **(B)** Representative image of an MDA-MB-231 spheroid with a compact aggregate morphology at day 6. **(C)** Immunostaining of MDA-MB-231 compact aggregates indicating nuclei (DAPI, blue), integrin $\alpha_v\beta_3$ (A488, green), collagen type I (APC, red), and the merged channels. **(D)** Diameter of HUVEC spheroids originated from 1×10^6 cells per mold after 1, 3, and 6 days of incubation. **(E)** Representative image of a HUVEC compact spheroid on day 6. **(F)** Immunostaining of HUVEC compact spheroids showing nuclei (DAPI, blue), integrin $\alpha_v\beta_3$ (A488, green), collagen type I (APC, red), and the merged channels. Scale bars: 200 μm *$p < 0.05$. (For interpretation of the references to colour in this figure legend, the reader is referred to the Web version of this article.)

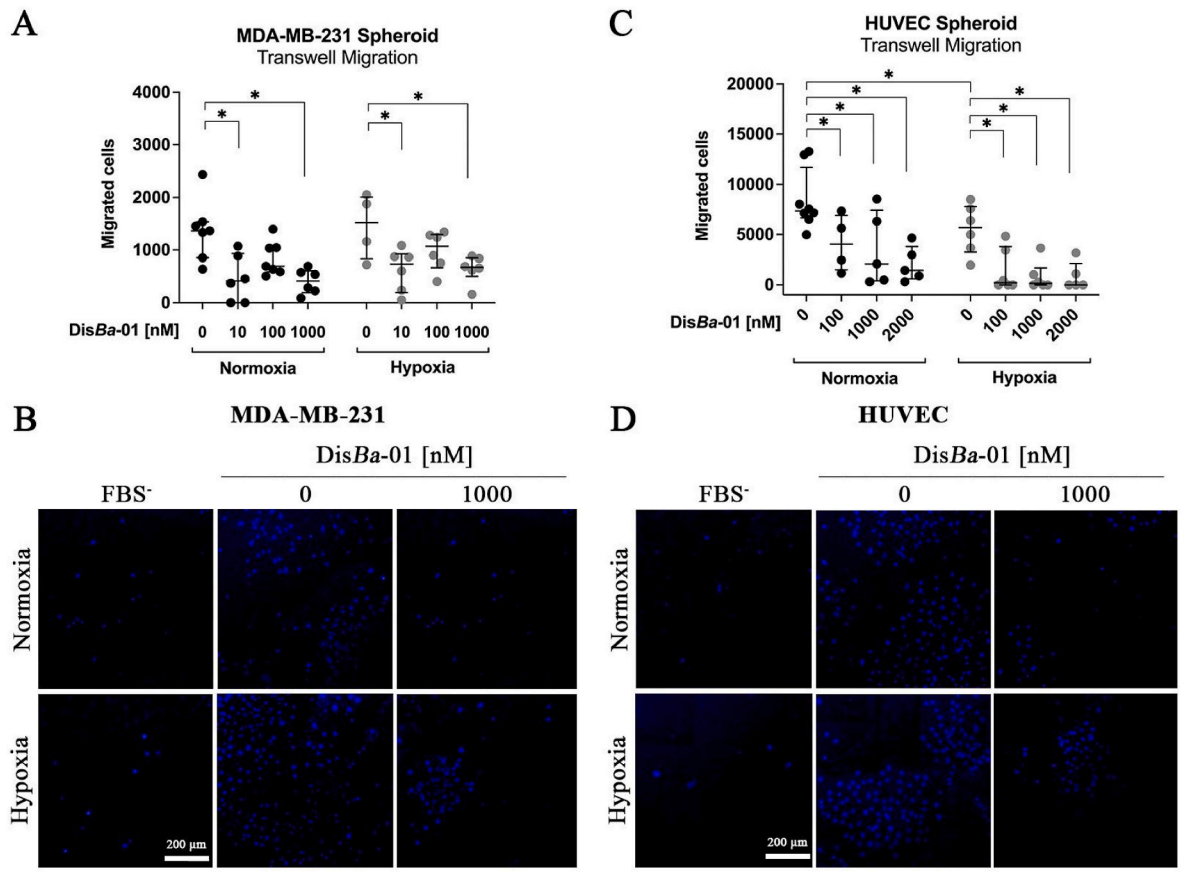

Fig. 2. Inhibition of spheroid migration after 24h of Dis*Ba*-01 treatment. (A) Quantification of migrated MDA-MB-231 cells after 24 h of treatment with Dis*Ba*-01 (10, 100, or 1000 nM), in normoxia (black) and hypoxia (grey). **(B)** Density of nuclei after 24 h of migration in a transwell system for MDA-MB-231 compact aggregates. **(C)** Quantification of migrated HUVEC cells after 24 h of treatment with Dis*Ba*-01 (100, 1000, or 2000 nM), in normoxia (black) and hypoxia (grey). **(D)** Density of nuclei after 24 h of migration in a transwell system for HUVEC compact spheroids. Scale bars: 200 µm *$p < 0.05$.

MDA-MB-231 compact aggregates displayed a lower expression of integrin $\alpha_v\beta_3$ than HUVEC compact spheroids, both in normoxia and hypoxia (Fig. 3A–C). HUVEC compact spheroids showed increased collagen type I secretion in comparison with MDA-MB-231 compact aggregates, both in normoxic and hypoxic conditions (Fig. 3B and C). Interestingly, neither integrin $\alpha_v\beta_3$ expression nor collagen type I secretion were altered by changes in oxygenation within a cell line. Overall, these results indicate that the oxygen concentration in 3D culture does not influence the levels of integrin $\alpha_v\beta_3$ expression, nor does it alter collagen type I deposition in spheroids.

3.4. *HUVEC spheroid sprouting in collagen type I is reduced by DisBa-01*

To understand how the blockage of integrin $\alpha_v\beta_3$ modulates sprout formation in endothelial cells grown in a spheroid setting, therefore mimicking an initial step essential for angiogenesis, we treated HUVEC spheroids with Dis*Ba*-01 (1 µM) and checked sprouts over 72 h. This assay was conducted only under normal oxygen levels and was aided by a collagen type I coating. Dis*Ba*-01 decreased the sprouting index, i.e. the sum of the length of sprouts normalized by the number of sprouts, after 24 h (42.19%, $p < 0.05$), 48 h (38.56%, $p < 0.05$) and 72 h (58.91%, $p < 0.05$) (Fig. 4A). It also reduced the number of sprouts observed per spheroid, from 6.30 ± 3.06 to 2.06 ± 1.91 after 24 h, from 4.96 ± 2.39 to 3.09 ± 4.76 after 48 h, and from 4.48 ± 2.88 to 2.67 ± 1.99 after 72 h (Fig. 4B). The loss of sprouting is visible in spheroids treated with Dis*Ba*-01 upon light microscopy when compared to the untreated control (Fig. 4C).

The distribution of VE-cadherin in endothelial cells is essential for sprouting due to its dynamic and intimate relationship with the F-actin cytoskeleton in tight junctions. In normoxia, Dis*Ba*-01 blockage of integrin $\alpha_v\beta_3$ diminished significantly VE-cadherin expression (Fig. 4D). Hypoxia alone was sufficient to reduce VE-cadherin distribution to basal levels, and Dis*Ba*-01 treatment did not add to this behavior (Fig. 4E). The staining control, consisting of secondary antibody staining, indicates the threshold levels of fluorescence observed in each oxygen condition (Fig. 4F).

4. Discussion

Three-dimensional culture brings an attractive approach to the study of the tumor microenvironment *in vitro*, allowing for the creation of structures with architecture and function similar to those found in tumor masses *in vivo* [6]. These 3D structures help us to understand better the role of the extracellular matrix, microfluidics, response to drugs, and cell-cell interactions when compared with standard cell culture [7,8]. It also allows us to better comprehend the role of adhesion molecules such as integrins in tumor development and response to treatment without the limitations of traditional 2D assays [9,10].

In this work, we established the basics of 3D cell culture for two lineages with importance for cancer research (HUVEC and MDA-MB-231), using a non-adhesive micromold method. The addition of Matrigel was crucial for constructing spheroids in both cell lines – in HUVECs, exogenous matrix absence caused cell death, and in MDA-MB-231 it led to the spreading of non-adherent cells - differently from what has been reported for MCF-7 [11]. Although both MDA-MB-231 and MCF-7 are breast adenocarcinoma strains, their differential expression of ER, PR, and HER2 receptors may interfere with multiple pathways within cells and generate distinct characteristics, such as the inability of

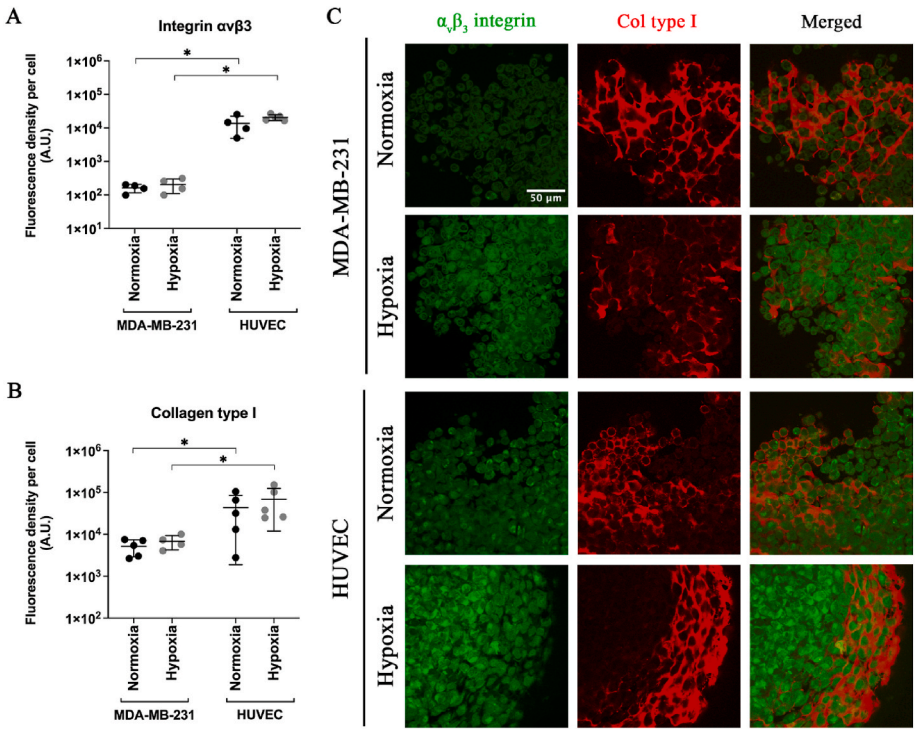

Fig. 3. Immunofluorescence of integrin $\alpha_v\beta_3$ and collagen type I in spheroids. (A) Fluorescence density of integrin $\alpha_v\beta_3$ in spheroids from MDA-MB-231 and HUVEC grown under normoxia (black) or hypoxia (grey), normalized per cell. **(B)** Fluorescence density of collagen type I in spheroids from MDA-MB-231 and HUVEC grown under normoxia (black) or hypoxia (grey), normalized per cell. **(C)** Representative images of cells from MDA-MB-231 and HUVEC spheroids grown under normoxia or hypoxia, stained for integrin $\alpha_v\beta_3$ (A488, green) and collagen type I (APC, red). Composition images are displayed on the far right. Scale bar: 20 μm $^*p <$ 0.05. (For interpretation of the references to colour in this figure legend, the reader is referred to the Web version of this article.)

MDA-MB-231 to self-assemble into spheroids. Interestingly, we observed that, from the gradient of compaction available for spheroids, our tumoral strain reached only the compact aggregate level, whereas the HUVEC spheroid developed the dense setting of a compact spheroid. The level of compaction may involve integrins such as the β_1 subunit, and a previous study correlated the formation of TNBC spheroids with the β_5 subunit and Src pathway, which led to adhesion and migration in both 2D and 3D models [12,13].

The use of MDA-MB-231 and HUVEC cell lines for spheroid migration follows up on earlier investigations of our research group, in which we evaluated the Dis*Ba*-01 mechanism of action in angiogenic signaling [3] and migratory response in normoxia and hypoxia [2]. Previous studies from our group found that Dis*Ba*-01, a recombinant disintegrin from *Bothrops alternatus* snake venom, binds preferentially with integrin $\alpha_v\beta_3$ [3] and inhibits directional migration of oral squamous sarcoma [4]. Moreover, the migration of MDA-MB-231 cells in hypoxia after Dis*Ba*-01 exposure was also lower, indicating an oxygen-independent mechanism of blocking directional motility [2]. Due to the similarities between our findings, we suggest the results obtained from traditional cell culture can be translated into 3D culture and, in the case of Dis*Ba*-01 exposure, elicit similar inhibitory mechanisms to previous studies.

It is noteworthy that Dis*Ba*-01 treatment in HUVEC and MDA-MB-231 spheroids required different disintegrin concentrations to trigger high levels of inhibition. The TNBC cell line was more sensitive to its effects, contrary to what was observed in 2D cultures, despite having the lower amount of integrin $\alpha_v\beta_3$ out of the two [2]. HUVECs have been described as sensitive to Dis*Ba*-01 activity as well, although responses seem to be exacerbated whenever VEGF is present in the system, likely due to the cross-talk between integrin $\alpha_v\beta_3$ and VEGFR2 [3]. Since we did not use VEGF as a supplement in the HUVEC spheroid culture, we upped the concentration of Dis*Ba*-01 to 2000 nM to generate higher migratory inhibition and, therefore, be able to compare both settings. We also tested whether Dis*Ba*-01 binds to VEGFR2 using surface plasmon resonance and found that the disintegrin binds 10 times more specifically to integrin $\alpha_v\beta_3$ than to VEGFR2 ().

The use of spheroids created from endothelial cells also supports the in-depth study of tumoral angiogenesis, particularly the sprouting of new vessels from an initial cell cluster. In this process, endothelial cells undergo remodeling and proliferation, and several proteins play a great role in stabilizing and destabilizing tight junctions and actin polarization to enable cell motility and ECM deposition [14,15]. The role of VE-cadherin in tumoral angiogenesis is essential: its moderate down-regulation enables the transient formation of actin-driven protrusions of the membrane named junction-associated intermittent lamellipodia (JAIL), which in turn induces new VE-cadherin adhesion sites and modulates, *in tandem*, both VE-cadherin binding and F-actin remodeling [14]. VE-cadherin also stabilizes the endothelial phenotype and allows for cell plasticity [1]. Once actin polarization is achieved, cells form a migratory tip that guides collective migration using adhesive molecules such as integrins $\alpha_v\beta_3$, $\alpha_v\beta_5$, $\alpha_5\beta_1$ [16].

In our work, we demonstrated that HUVEC spheroids have a high concentration of integrin $\alpha_v\beta_3$ and secrete abundant levels of collagen type I, indicating the supportive role of endothelial cells in the tumor microenvironment. Interestingly, the expression levels of both proteins remain stable under oxidative stress due to hypoxia, indicating these processes may have an oxygen-independent regulation. Investigating VE-cadherin, we observed that hypoxia alone is sufficient to down-regulate its levels to a basal threshold, which is also obtained through the blockage of integrin $\alpha_v\beta_3$ by Dis*Ba*-01. Moreover, spheroids under normal oxygen conditions show a significant decrease in sprout size and number after Dis*Ba*-01 treatment, which indicates the role of integrin $\alpha_v\beta_3$ in sprout formation and cements the disintegrin as an important angiogenesis inhibitor.

Our work has limitations, including (1) the investigation of a single TNBC cell line as opposed to multiple breast cancer lineages, (2) the mechanism of spheroid migration, particularly in hypoxia, where cell

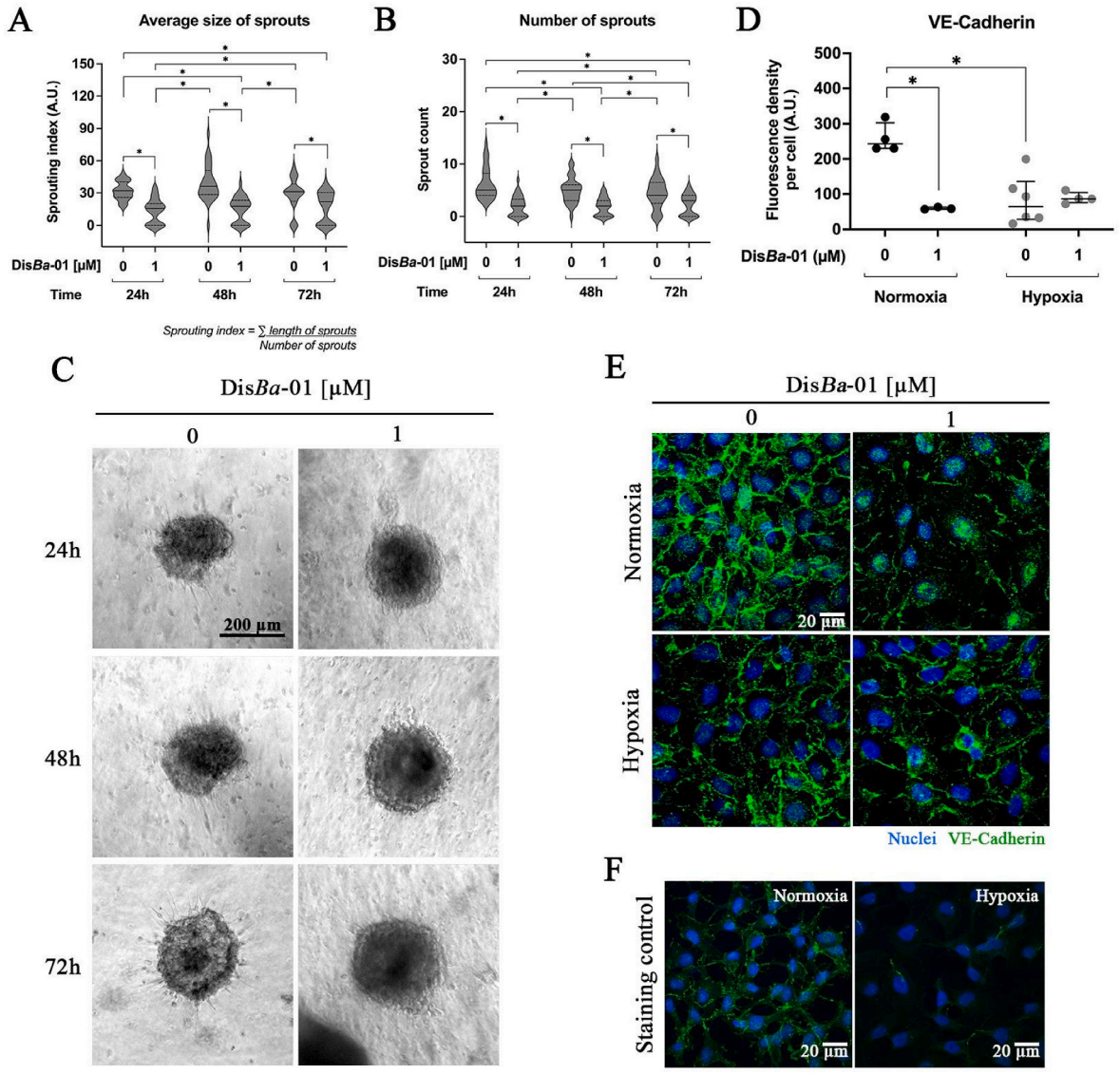

Fig. 4. HUVEC spheroid sprouting in collagen type I coating after Dis*Ba*-01 treatment. (A) Average size of sprouts obtained from the sum of the length of sprouts divided by the number of sprouts. Spheroids were treated with Dis*Ba*-01 (1 µM) for 24, 48, and 72 h before measurement. **(B)** Number of sprouts of each spheroid after treatment with Dis*Ba*-01 (1 µM) throughout 72 h. **(C)** Representative images of sprouts from untreated spheroids (0, left) compared with Dis*Ba*-01-treated spheroids (1000 nM, right) after 24, 48 and 72 h. Scale bar: 200 µm. **(D)** Quantification of VE-cadherin fluorescence density per cell after spheroid treatment with Dis*Ba*-01 in normoxia (black) and hypoxia (grey). **(E)** Confocal microscopy images of HUVEC spheroids upon Dis*Ba*-01 treatment in normoxia and hypoxia, stained for VE-cadherin (A488, green) and DAPI (blue). Scale bar: 20 µm. **(F)** Secondary antibody (A488) staining control for spheroids in normoxia and hypoxia. Nuclei stained with DAPI (blue). Scale bar: 20 µm $^*p < 0.05$. (For interpretation of the references to colour in this figure legend, the reader is referred to the Web version of this article.)

adhesion properties are compromised, (3) the use of a single method for spheroid formation, considering the various methods available, such as hanging drop and gel embedding [17]. We have also observed the lack of sprouting from HUVEC spheroids in hypoxia regardless of Dis*Ba*-01 presence, despite the known increase in VEGF secretion under low oxygen levels and that Dis*Ba*-01 can block the VEGFR2 cross-talk with integrin $\alpha_v\beta_3$ in VEGF presence [3,18]. Those circumstances pend investigation to improve our knowledge over *in vitro* models of metastatic cancer.

5. Conclusion

We demonstrated that the integrin $\alpha_v\beta_3$ inhibition by Dis*Ba*-01 promotes similar results to those found in traditional cell culture assays, indicating that certain results from 2D culture may be upscaled to 3D culture successfully. Spheroids from HUVEC show increased levels of integrin $\alpha_v\beta_3$ expression and collagen type I secretion compared with the ones from MDA-MB-231, which denotes their supportive role in the tumor microenvironment. Dis*Ba*-01 was also shown to interfere with HUVEC sprouting, inhibiting the number and length of sprouts and down-regulating VE-cadherin expression. Overall, our data demonstrates for the first time the anti-angiogenic role of Dis*Ba*-01 in 3D cell culture, validating its anti-tumoral potential.

Funding

This work was supported by the São Paulo Research Foundation (grant numbers: 2021/01983-4; 2019/11437-7) and the Coordenação de Aperfeiçoamento de Pessoal de Nível Superior - Brasil (CAPES; grant number: 001).

CRediT authorship contribution statement

Bruna Carla Casali: Writing – original draft, Validation, Methodology, Formal analysis, Data curation. **Matheus Pintor Baptista:** Validation, Investigation, Formal analysis. **Bianca Cruz Pachane:** Writing – review & editing, Validation, Software, Data curation. **Anelise Abreu Cortez:** Methodology, Formal analysis. **Wanessa Fernanda Altei:** Writing – review & editing, Visualization, Supervision, Methodology, Formal analysis, Conceptualization. **Heloísa Sobreiro Selistre-de-Araújo:** Writing – review & editing, Supervision, Project administration, Funding acquisition, Data curation, Conceptualization.

Declaration of competing interest

The authors declare that they have no known competing financial interests or personal relationships that could have appeared to influence the work reported in this paper.

Data availability

Data will be made available on request.

Appendix A. Supplementary data

Supplementary data to this article can be found online at https://doi.org/10.1016/j.bbrep.2024.101686.

References

[1] K.J. Choi, J.-K. Nam, J.-H. Kim, S.-H. Choi, Y.-J. Lee, Endothelial-to-mesenchymal transition in anticancer therapy and normal tissue damage, Exp. Mol. Med. 52 (2020) 781–792, https://doi.org/10.1038/s12276-020-0439-4.

[2] B.C. Casali, L.T. Gozzer, M.P. Baptista, W.F. Altei, H.S. Selistre-de-Araújo, The effects of αvβ3 integrin blockage in breast tumor and endothelial cells under hypoxia in vitro, Int. J. Mol. Sci. 23 (2022) 1745, https://doi.org/10.3390/ijms23031745.

[3] T.M. Danilucci, P.K. Santos, B.C. Pachane, G.F.D. Pisani, R.L.B. Lino, B.C. Casali, W. F. Altei, H.S. Selistre-de-Araujo, Recombinant RGD-disintegrin DisBa-01 blocks integrin αvβ3 and impairs VEGF signaling in endothelial cells, Cell Commun. Signal. 17 (2019) 27, https://doi.org/10.1186/s12964-019-0339-1.

[4] C.F. Montenegro, B.C. Casali, R.L.B. Lino, B.C. Pachane, P.K. Santos, A.R. Horwitz, H.S. Selistre-de-Araujo, M.L. Lamers, Inhibition of αvβ3 integrin induces loss of cell directionality of oral squamous carcinoma cells (OSCC), PLoS One 12 (2017) e0176226, https://doi.org/10.1371/journal.pone.0176226.

[5] O.H.P. Ramos, A. Kauskot, M.R. Cominetti, I. Bechyne, C.L. Salla Pontes, F. Chareyre, J. Manent, R. Vassy, M. Giovannini, C. Legrand, H.S. Selistre-de-Araujo, M. Crépin, A. Bonnefoy, A novel alpha(v)beta (3)-blocking disintegrin containing the RGD motive, DisBa-01, inhibits bFGF-induced angiogenesis and melanoma metastasis, Clin. Exp. Metastasis 25 (2008) 53–64, https://doi.org/10.1007/s10585-007-9101-y.

[6] H. Özkan, D.G. Öztürk, G. Korkmaz, Transcriptional factor repertoire of breast cancer in 3D cell culture models, Cancers 14 (2022) 1023, https://doi.org/10.3390/cancers14041023.

[7] S.J. Han, S. Kwon, K.S. Kim, Challenges of applying multicellular tumor spheroids in preclinical phase, Cancer Cell Int. 21 (2021) 152, https://doi.org/10.1186/s12935-021-01853-8.

[8] M. Stadler, S. Walter, A. Walzl, N. Kramer, C. Unger, M. Scherzer, D. Unterleuthner, M. Hengstschläger, G. Krupitza, H. Dolznig, Increased complexity in carcinomas: analyzing and modeling the interaction of human cancer cells with their microenvironment, Semin. Cancer Biol. 35 (2015) 107–124, https://doi.org/10.1016/j.semcancer.2015.08.007.

[9] C.-Y. Su, J.-Q. Li, L.-L. Zhang, H. Wang, F.-H. Wang, Y.-W. Tao, Y.-Q. Wang, Q.-R. Guo, J.-J. Li, Y. Liu, Y.-Y. Yan, J.-Y. Zhang, The biological functions and clinical applications of integrins in cancers, Front. Pharmacol. 11 (2020) 579068, https://doi.org/10.3389/fphar.2020.579068.

[10] Y. Fang, S. Liang, J. Gao, Z. Wang, C. Li, R. Wang, W. Yu, Extracellular matrix stiffness mediates radiosensitivity in a 3D nasopharyngeal carcinoma model, Cancer Cell Int. 22 (1) (2022 Nov 19) 364, https://doi.org/10.1186/s12935-022-02787-5.

[11] K. Froehlich, J.-D. Haeger, J. Heger, J. Pastuschek, S.M. Photini, Y. Yan, A. Lupp, C. Pfarrer, R. Mrowka, E. Schleußner, U.R. Markert, A. Schmidt, Generation of multicellular breast cancer tumor spheroids: comparison of different protocols, J. Mammary Gland Biol. Neoplasia 21 (2016) 89–98, https://doi.org/10.1007/s10911-016-9359-2.

[12] G.A. Howe, C.L. Addison, β1 integrin: an emerging player in the modulation of tumorigenesis and response to therapy, Cell Adhes. Migrat. 6 (2012) 71–77, https://doi.org/10.4161/cam.20077.

[13] H.-J. Park, D.M. Helfman, Up-regulated fibronectin in 3D culture facilitates spreading of triple negative breast cancer cells on 2D through integrin β-5 and Src, Sci. Rep. 9 (2019) 19950, https://doi.org/10.1038/s41598-019-56276-3.

[14] J. Cao, M. Ehling, S. März, J. Seebach, K. Tarbashevich, T. Sixta, M.E. Pitulescu, A.-C. Werner, B. Flach, E. Montanez, E. Raz, R.H. Adams, H. Schnittler, Polarized actin and VE-cadherin dynamics regulate junctional remodelling and cell migration during sprouting angiogenesis, Nat. Commun. 8 (2017) 2210, https://doi.org/10.1038/s41467-017-02373-8.

[15] J.A. Harry, M.L. Ormiston, Novel pathways for targeting tumor angiogenesis in metastatic breast cancer, Front. Oncol. 11 (2021) 772305, https://doi.org/10.3389/fonc.2021.772305.

[16] R. Silva, G. D'Amico, K.M. Hodivala-Dilke, L.E. Reynolds, Integrins: the keys to unlocking angiogenesis, ATVB 28 (2008) 1703–1713, https://doi.org/10.1161/ATVBAHA.108.172015.

[17] G.Y. Lee, P.A. Kenny, E.H. Lee, M.J. Bissell, Three-dimensional culture models of normal and malignant breast epithelial cells, Nat. Methods 4 (2007) 359–365, https://doi.org/10.1038/nmeth1015.

[18] D. Rodriguez, D. Watts, D. Gaete, S. Sormendi, B. Wielockx, Hypoxia pathway proteins and their impact on the blood vasculature, IJMS 22 (2021) 9191, https://doi.org/10.3390/ijms22179191.